THE JOURNAL OF PHYSICAL CHEMISTRY C

Article

Cite This: J. Phys. Chem. C XXXX, XXX, XXX–XXX

pubs.acs.org/JPCC

Dynamic Evolution of 2D Layers within Perovskite Nanocrystals via Salt Pair Extraction and Reinsertion

Lance M. Wheeler,*[,†] Nicholas C. Anderson,[†] Taylor S. Bliss,[†,‡] Matthew P. Hautzinger,[†,§,∥] and Nathan R. Neale*[,†]

[†]Chemistry and Nanoscience Center, National Renewable Energy Laboratory, Golden, Colorado 80401, United States

[‡]Department of Chemical Engineering, University of Florida, Gainesville, Florida 32611, United States

[§]Department of Chemistry, University of Southern Illinois, Carbondale, Illinois 62901, United States

Supporting Information

ABSTRACT: Metal halide perovskite (MHP) semiconductors exhibit unprecedented optoelectronic properties coupled with low formation energies that enable scalable, cost-efficient solution processing. The low formation energies additionally facilitate dynamic transformation of the chemical composition and crystal structure of the MHP material. In this work, we show that CsBr salt is selectively extracted from $CsPbBr_3$ nanocrystals (NCs) to yield $PbBr_2$ NCs. The $PbBr_2$ NCs are then exposed to different glacial acetic acid ABr salt solutions to generate a variety of emissive compounds with the generic structure $A'_2A_{n-1}Pb_nBr_{3n-1}X'_2$, where A = cesium ($Cs^+$), methylammonium ($MA^+$), formamidinium ($FA^+$); A′ = A or H^+; X′ = Br^- or acetate (CH_3COO^-); and n is the number of lead halide layers, where n = 1, 2, 3, ...∞. We systematically vary the ratios of $PbBr_2$/ABr/CH_3COOH and show that certain ratios result in isolable single-phase $APbBr_3$ NCs—an effective A-site cation exchange from the parent $CsPbBr_3$ NCs. Importantly, time-resolved photoluminescence (PL) spectroscopy shows the dynamic evolution of many additional species as evidenced by blue-shifted emission peaks from 2.85−2.49 eV for MA^+-based structures. We assign these species to n = 1, 2, 3, 4, and 5 quasi-two-dimensional network (2DN) sheets, in which CH_3COO^- anions and Br^- anions compete for the c-axis X′ sites separating haloplumbate(II) layers within the $A'_2A_{n-1}Pb_nBr_{3n-1}X'_2$ NCs. Finally, we demonstrate the degree of CH_3COO^- incorporation, and thus the 2DN layer thickness and PL energy, is controlled in the early reaction times by kinetic factors. After a longer time (3 h), thermodynamic forces dictated by Le Chatelier's principle tune the structure in $A'_2A_{n-1}Pb_nBr_{3n-1}X'_2$ NCs from exclusively n = 1 to n = ∞ depending on the $PbBr_2$/ABr/CH_3COOH ratio.

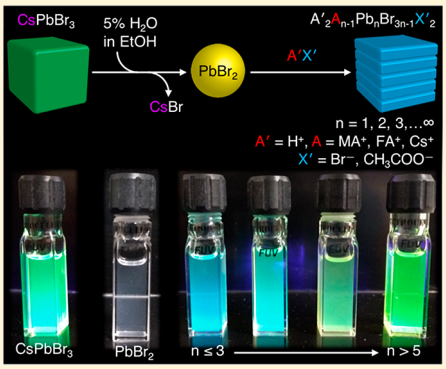

INTRODUCTION

In less than a decade, metal halide perovskite (MHP) semiconductors have risen to prominence as a material with unprecedented performance in optoelectronic technologies for photon conversion and emission.[1] Thin film MHP solar cells have reached stable solar power conversion efficiencies[2] that rival conventional photovoltaic technologies,[3] and the rapid development of MHP nanocrystals (NCs) have established these nanostructures as promising top cells of a tandem solar cell.[4] Additionally, MHP NCs show narrow emission line widths critical for lighting and display applications,[5] they provide the first example of a nonorganic material with efficient triplet emission,[6] and they reportedly exhibit near-unity quantum yield (QY)[7−9] even in the absence of complex, passivating shells typically required for high QY in metal chalcogenide and III−V NC emitter materials.[10]

The emissive properties of MHP NCs have been manipulated in numerous ways. MHP NCs below ∼10 nm diameter display blue-shifted emission due to quantum confinement effects.[11,12] NCs also kinetically trap crystalline phases with favorable optical properties that are not thermodynamically favored at larger scales.[11] The low formation energies of MHPs[12] allow for an array of low-temperature chemical transformations to the perovskite structure,[13] which features octahedra, MX_6^{4-}, composed of a divalent metal (M^{2+}) coordinated with six halide anions (X^-). The halide anions rapidly exchange in solution to yield widely tunable bandgaps with emission energies spanning the visible spectrum.[14−16] There are examples of cation exchange of the M-site as well, where Sn^{2+} is swapped for Pb^{2+} in thin film perovskites.[17] Partial M-site exchange with Sn^{2+}, Cd^{2+}, and Zn^{2+} has been achieved in NCs that demonstrate blue-shifted emission due to contraction of the crystal lattice from the parent Pb^{2+}-based NCs.[18] Red-shifted emission is observed in MHP NCs with M-sites exchanged for Mn^{2+}.[19]

In a MHP crystal, the negative charge of metal halide octahedra is balanced by monovalent cations such as alkali

Special Issue: Prashant V. Kamat Festschrift

Received: February 1, 2018
Revised: April 27, 2018
Published: April 28, 2018

DOI: 10.1021/acs.jpcc.8b01164
J. Phys. Chem. C XXXX, XXX, XXX–XXX

metals or organic cations. The size of the cations influences the emission properties by changing the bonding, dimensionality, and tilt angle of the metal halide octahedra. Cations with ionic radii that satisfy the geometric "tolerance factor"[20] will form three-dimensional, isotropic crystals with the general crystal structure AMX_3, where A is commonly cesium (Cs^+), methylammonium (MA^+), and formamidinium (FA^+). Exchange of MA^+ for FA^+ has been shown for thin films through a solution process[21] and in NCs through a solid−liquid−solid process.[22] Larger cations lead to layered compounds with blue-shifted emission due to quasi-two-dimensional network (2DN) quantum confinement.[23−27]

In addition to the metal ion, A-site cation, and halide anion exchange reactions, there are several examples of postsynthetic reactions to insert or remove ion pairs from NC lattices that have been successful in tuning emission properties. For example, nonemissive Cs_4PbX_6 NCs (X = Cl^-, Br^-, I^-) have been transformed into brightly luminescent $CsPbBr_3$ using physical and chemical extraction of CsBr.[28,29] Other works have reported the inverse transformation from $CsPbBr_3$ to $Cs_4Pb_2Br_6$ with the addition of $PbBr_2$.[28,29] PbI_2 NCs have been shown to react with (MA)I to form $(MA)PbI_3$ NCs.[30] $CsPbBr_3$ NCs have also been transformed into 2DN $CsPb_2Br_5$ nanosheets using solution ligand chemistry.[31] $CsPbBr_3$ NCs have been synthesized using CsX[32] and metallic Pb[33] NCs as synthons by adding the remaining components to the solution at room temperature.

In this work, we extend the breadth of salt pair extraction and insertion reactions by demonstrating the ability to utilize $CsPbBr_3$ NCs as a synthon to cation-exchanged $APbBr_3$ NCs as well as 2DN layered perovskites within the original NC framework. These transformations are achieved by converting $CsPbBr_3$ NCs into $PbBr_2$ NCs by extracting CsBr with a water−ethanol solution. We subsequently reinsert ion pairs into the $PbBr_2$ NCs to yield an array of compounds with the generic structure of $A'_2A_{n-1}Pb_nBr_{3n-1}X'_2$, where A = Cs^+, MA^+, FA^+; A′ = A or H^+; X′ = Br^- or acetate (CH_3COO^-); and n is the thickness of the 2DN sheet, where n = 1, 2, 3, ...∞. Depending on the conditions, we demonstrate NC solutions with similar size and emission properties to the parent $CsPbBr_3$ NCs, showing that the salt extraction and reinsertion processes do not disrupt the $PbBr_2$ NC framework. We also spectroscopically characterize kinetically stable compounds with blue-shifted emission due to the formation of 2DN quantum-confined sheets, in which CH_3COO^- and Br^- anions compete for the c-axis X′ sites in $A'_2A_{n-1}Pb_nBr_{3n-1}X'_2$ NCs. The larger size of X′ = CH_3COO^- vs Br^- disrupts the three-dimensional (3D) MHP NC lattice and results in 2DN sheets exhibiting blue-shifted emission relative to their 3D counterparts. We demonstrate the degree of CH_3COO^- incorporation, and thus, the 2DN layer thickness and emission energy, is tuned both by kinetics and thermodynamics (the latter using Le Chatelier's Principle) from exclusively n = 1 to n = ∞ in the $A'_2A_{n-1}Pb_nBr_{3n-1}X'_2$ structure. This approach highlights both the benefits and challenges associated with the solution environment of perovskite NCs and enables chemistries inaccessible in conventional synthetic strategies of nanostructured and bulk perovskites.

EXPERIMENTAL METHODS

Cs-Oleate Precursor Synthesis. $CsCO_3$ (814 mg, 2.50 mmol, Aldrich, ReagentPlus, 99%), octadecene (ODE, 40 mL, Aldrich, Technical grade, 90%), and oleic acid (2.5 mL, 7.9 mmol, Aldrich, Technical grade, 90%) were placed in a 250 mL round-bottom flask (RBF). The mixture was heated under vacuum (10^{-2} Torr) at 120 °C for 1 h and then at 150 °C under N_2 while stirring with a magnetic stir bar. Heating was continued until a transparent, colorless solution was formed (∼20 min). The temperature of the solution was 100 °C for injection.

$PbBr_2$ Precursor Synthesis. A total of 0.274 g of $PbBr_2$ (Aldrich, ≥ 98%) and 30 mL of ODE were placed in a separate RBF. The mixture was dried under vacuum by heating at 120 °C for 1 h while stirring with a magnetic stir bar. Under N_2, 2 mL of dry oleylamine (Aldrich, Technical grade, 70%) and 2 mL of oleic acid were injected through the septum using a syringe. Oleylamine and oleic acid were dried using 3 Å molecular sieves. After all of the bulk $PbBr_2$ reacted, a transparent, colorless solution formed, at which point the temperature was raised to 170 °C.

$CsPbBr_3$ NC Synthesis. A volume of 1.6 mL of the 100 °C Cs-oleate precursor was injected with a syringe through a septum into the 170 °C $PbBr_2$ precursor to yield a bright yellow solution. The RBF was immediately removed from heat, and the reaction was quenched using an ice bath. The solution turned green and brightly luminescent upon cooling. When the temperature of the solution reached 30 °C, the $CsPbBr_3$ NC solution was transferred to a centrifuge tube, and the $CsPbBr_3$ NC solution was centrifuged at 10 000g for 3 min. The light green supernatant was discarded, and the $CsPbBr_3$ NCs were dispersed in hexanes (∼10 mL) and then centrifuged again at 6600g for 3 min. The green solids were discarded and the supernatant was collected. An antisolvent solution was formed by combining 1.6 mL of oleic acid and 1.6 mL of oleylamine with 37.5 mL of acetone. A volume of 20 mL of the antisolvent solution was used to precipitate the NCs from the hexane solution, and the cloudy suspension was centrifuged at 10 000g for 3 min. The transparent, colorless supernatant was discarded, leaving a green precipitate.

$PbBr_2$ NC Preparation. A CsBr extraction solution was formed by combining 9 mL of ethanol (dried over 3 Å molecular sieves), 0.75 mL of dry oleylamine, and 0.25 mL of dry oleic acid, and 0.40 mL of deionized water. We found that the variable amounts of water present in nondried reagents did not provide reproducible results, and a known amount of water had to be added to successfully achieve $PbBr_2$ NCs. The extraction solution was added to the solid $CsPbBr_3$ NCs and shaken or sonicated until the green powder turned white. Remaining $CsPbBr_3$ NCs were easily identified by green emission under UV illumination; if green emission was observed, additional shaking or sonication was performed. The resulting cloudy, colorless mixture was centrifuged at 10 000g for 3 min, and the supernatant was discarded. The process may also be carried out on $PbBr_2$ NCs by adding the extraction solution to $CsPbBr_3$ NCs solvated in 10 mL of hexane. In this case, the NCs precipitate out of solution, and the mixture turns cloudy and colorless within 3 to 4 min. After turning colorless, the mixture was centrifuged at 10 000g for 3 min. The solid $PbBr_2$ NCs were solvated in 10 mL of dry toluene to yield a colorless solution. $PbBr_2$ NC solutions were stored on a Schlenk line under N_2 until they were used for further transformations.

X-ray Diffraction. XRD measurements were performed on a Bruker D8 Discover X-ray Diffraction system with a 2.2 kW sealed Cu X-ray source. Patterns were acquired by depositing precipitated NCs onto a glass slide and scanning over 2θ using a beam voltage and current of 40 kV and 35 mA, respectively.

DOI: 10.1021/acs.jpcc.8b01164
J. Phys. Chem. C XXXX, XXX, XXX−XXX

Simulated powder diffraction patterns were generated using VESTA version 3.4 with .cif files from references 34−36.

$A'_2A_{n-1}Pb_nBr_{3n-1}X'_2$ NC Synthesis. ABr salt solutions (0.01 M) were prepared in glacial acetic acid. First, 1.0 mL of the 0.01 M ABr solution was combined with 0.1−0.25 mL of oleylamine and 0.1−0.25 mL of oleic acid and between 0−1 mL of acetic acid to form conversion stock solution. Then, 0.1 mL of the resulting stock solution was added to a cuvette and diluted with a known volume of toluene. The amount of toluene added depended on the amount of $PbBr_2$ NCs added in the next step, because it was used to keep the total volume constant at 2.5 mL. Between 0.1 and 2 mL of $PbBr_2$ NC solution in toluene was added to the toluene-diluted conversion stock solution (0.01 M solution of ABr with oleylamine, oleic acid, and acetic acid) to reach a final volume of 2.5 mL. The solution changes from transparent to light yellow upon addition of $PbBr_2$ NCs, which then evolves with time, depending on the conditions. Each reagent was stored over 3 Å molecular sieves overnight before use.

Transmission Electron Microscopy (TEM). Images were acquired on an FEI ST30 TEM operated at 300 kV. Samples were prepared by dropping dilute toluene solutions of NCs onto ultrathin carbon film/holey carbon, 400 mesh copper TEM grids. To remove excess ligands and obtain higher-resolution images, the samples were washed by dripping neat hexane onto the grid.

Fourier Transform Infrared Spectroscopy (FTIR). Spectra were acquired on a Bruker Alpha FTIR spectrometer inside an Ar atmosphere glovebox. Spectra of NC samples were obtained in diffuse reflectance mode. Samples were prepared by depositing centrifuged powder onto an aluminum- or gold-coated Si wafer. Spectra were collected by averaging 50 scans at 2 cm^{-1} resolution. Spectra of neat oleic acid and oleylamine liquids were acquired in attenuated total reflectance mode on the same spectrometer by depositing a drop of the liquid onto a diamond ATR crystal and collecting spectra by averaging 50 scans at 2 cm^{-1} resolution.

Photoluminescence Spectroscopy. Emission measurements were acquired using an OceanOptics OceanFX fiber-optically coupled Silicon CCD array. The OceanFX was controlled with custom LabVIEW software that allows extremely long averaging times (from ms to h) while maintaining a correct dark signal by using a light on−off acquisition sequence with a shutter cycle time of a few hundred ms. A ThorLabs M405FP1 fiber coupled 405 nm LED provided the light source, controlled by a ThorLabs DC2200 high-power LED Driver. The typical output power after coupling through a single 1000 μm was around 250 mW, which was allowed to have two passes through the sample by the use of a mirror on the back side of the cuvette. The typical acquisition times for photoluminescence were an integration time of 100 ms and an averaging time of a few min. The spectral sensitivity of the detector was calibrated against the HL2000-HP tungsten halogen lamp, assuming it is a perfect blackbody with a temperature of 3000 K.

RESULTS AND DISCUSSION

$CsPbBr_3$ NCs are synthesized using the previously reported hot injection technique.[34] After the NCs are purified to remove excess reactants and size-selected using centrifugation, the NCs are treated to extract CsBr and yield $PbBr_2$ NCs (Scheme 1). Salt extraction is achieved by exploiting the selective solubility of CsBr versus $PbBr_2$ in a solution of wet ethanol (EtOH), oleic acid, and oleylamine (CsBr is highly soluble in water and alcohols, whereas $PbBr_2$ is not). The presence of oleylamine (8.3 vol %) and oleic acid (2.8 vol %) as well as water (5 vol %) in the hydrated ethanol solution are critical to maintain the $PbBr_2$ NCs during the process and not produce bulk $PbBr_2$. The process may be carried out on $PbBr_2$ NCs in the solid phase or by adding the extraction solution to $CsPbBr_3$ NCs solvated in hexane. In both cases, adding the extraction solution generates a cloudy (optically scattering), colorless $PbBr_2$ NC suspension, from which the $PbBr_2$ NCs can be easily separated via centrifugation. The resulting solid $PbBr_2$ NCs are soluble in nonpolar solvents such as hexane and toluene.

Scheme 1. Transformations of MHP NCs Based on CsBr Salt Extraction from $CsPbBr_3$ NCs to Form $PbBr_2$ NCs that Are Re-formed into $A'_2A_{n-1}Pb_nBr_{3n-1}X'_2$ NCs via A′X′ Addition[a]

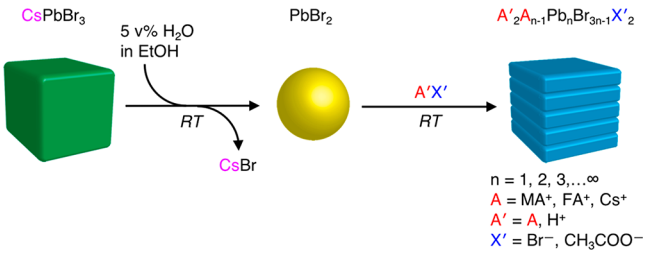

[a]A′ = A or H^+; A = cesium (Cs^+), methylammonium (MA^+), formamidinium (FA^+); X′ = Br^- or acetate (CH_3COO^-); and n is the thickness of the 2DN sheet, where n = 1, 2, 3, ...∞.

We characterize the optical, structural, and chemical properties of the NCs before and after removal of CsBr from the $CsPbBr_3$ lattice to confirm the effectiveness of the initial salt extraction step. $CsPbBr_3$ NCs exhibit a sharp absorption onset at 517 nm and a photoluminescence (PL) peak centered at 521 nm (2.38 eV) with a narrow full-width at half-maximum (fwhm) value of 82 meV (red spectra, Figure 1a). After CsBr extraction, the absorption onset of the $PbBr_2$ NCs is shifted to 330 nm, which is consistent with the bulk $PbBr_2$ bandgap of 3.9 eV. No PL was observed from the $PbBr_2$ NCs.

TEM images of a representative individual (Figure 1b) and an array of $CsPbBr_3$ NCs (Figure 1c) shows they are quasi-cubic in shape with dimensions in the range of 6−20 nm, consistent with the original report by Kovalenko and co-workers.[34] Upon CsBr salt extraction, the resulting $PbBr_2$ NCs are quasi-spheres that are 5−10 nm in diameter (Figure 1d,e). The reduction in crystallite size is due to loss of CsBr. X-ray diffraction (XRD) patterns confirm the transformation from $CsPbBr_3$ to $PbBr_2$ and reduction in crystallite size. The XRD pattern of the parent $CsPbBr_3$ NCs (red pattern, Figure 1f) exhibits the orthorhombic (*Pnma*) perovskite crystal phase, which is confirmed by the simulated pattern below the data.[35] Upon CsBr salt extraction, the powder XRD pattern from the resulting $PbBr_2$ NCs exhibits the expected orthorhombic (*Pmnb*) crystal structure[36] with broadened peaks (blue pattern, Figure 1f), consistent with Scherrer broadening for smaller crystallites.

We use Fourier transform infrared (FTIR) spectroscopy to gain insight on the chemical changes resulting from conversion of $CsPbBr_3$ to $PbBr_2$ NCs. The FTIR spectrum of the parent $CsPbBr_3$ NCs is dominated by resonances of the surface ligands (red spectrum, Figure 1g). The alkyl chains of the ligands are clearly identified by the characteristic modes from hydrocarbon

DOI: 10.1021/acs.jpcc.8b01164
J. Phys. Chem. C XXXX, XXX, XXX−XXX

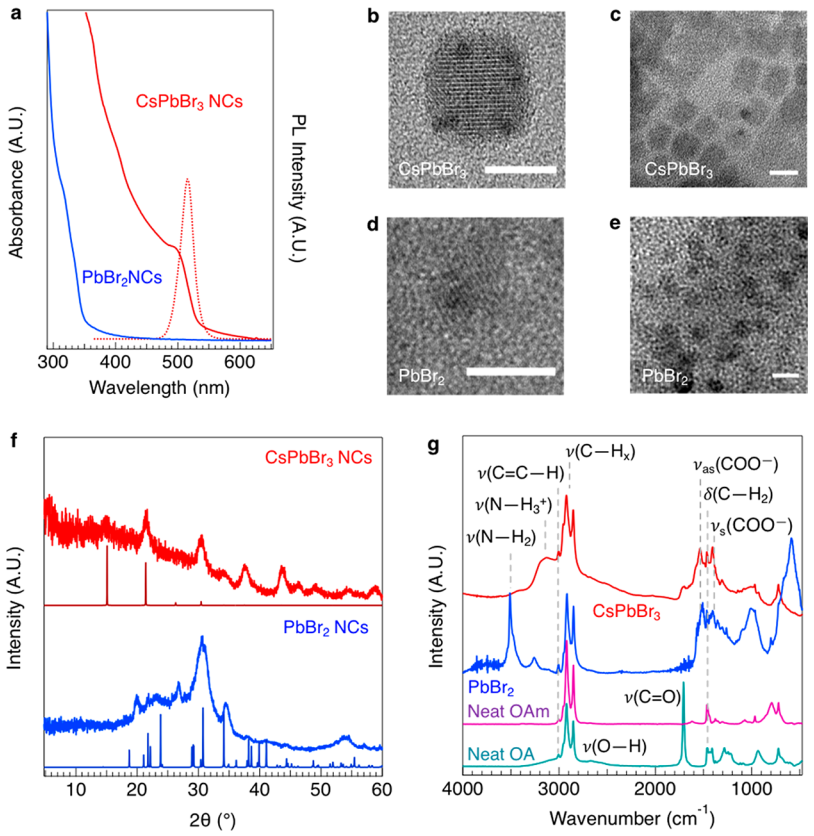

Figure 1. (a) Absorbance (solid) and emission (dashed) spectra, (b–e) TEM images, (f) XRD patterns, and (g) FTIR spectra of $CsPbBr_3$ and $PbBr_2$ NCs generated by CsBr salt extraction. In (a), $PbBr_2$ NCs do not emit. In (g), FTIR spectra of neat oleylamine (OAm) and oleyic acid (OA) are shown for reference.

stretching, $\nu(C{-}H_x)$ = 2925 cm^{-1}, and methylene deformation, $\delta(C{-}H_2)$ = 1464 cm^{-1}. Vinylic C–H resonances are also clearly observed at $\nu(C{=}C{-}H)$ = 3007 cm^{-1} resulting from oleyl groups in the ligand shell. The nature of ligand binding to the NC surface is apparent based on the peak centered at $\nu(N{-}H_3^+)$ = 3132 cm^{-1} (red spectrum, Figure 1g). This feature is due to stretching modes from oleylammonium, showing that the ligands are cationically charged to balance the negative surface termination of the lead halide octahedra or oleate ligands in the parent $CsPbBr_3$ NCs.[37] Oleylamine (OAm) is provided for reference (purple spectrum, Figure 1g). Oleic acid (OA) is present in excess relative to the $CsPbBr_3$ NCs that drives oleyl carboxylate (oleate) onto the NC surface, providing colloidal stability and preventing NC coalescence in solution.[37] The excess OA in the $CsPbBr_3$ NC spectrum is evidenced by the broad baseline from hydroxyl stretching spanning $\nu(O{-}H)$ = 2400–3400 cm^{-1} and the carbonyl at $\nu(C{=}O)$ = 1707 cm^{-1} of the carboxylic acid group, based on comparison to the neat OA spectrum (teal spectrum, Figure 1g). In addition, oleate ligands are easily identified by the absence of the broad hydroxyl peak and new peaks characteristic of carboxylate, which are the symmetric, $\nu_s(COO^-)$ = 1407 cm^{-1}, and asymmetric, $\nu_{as}(COO^-)$ = 1538 cm^{-1}, stretching modes. Thus, the ligand shell of isolated $CsPbBr_3$ NCs appears to comprise oleylammonium and oleate, with additional excess oleic acid coprecipitating with the NCs during isolation.

Upon extraction of CsBr, the FTIR spectrum of the resulting $PbBr_2$ NCs exhibits significantly different surface chemistry. An intense new resonance assigned to OAm, $\nu(N{-}H_2)$ = 3511 cm^{-1}, suggests that OAm binds to Pb surface atoms as a neutral L-type ligand[38] (blue spectrum, Figure 1g), as expected for this compound. The $PbBr_2$ NCs also are free from excess OA based on the absence of $\nu(C{=}O)$ = 1707 cm^{-1} of the carboxylic acid group. A small feature at ~3250 cm^{-1} is likely due to the $\nu(N{-}H_3^+)$ stretch from a charge-balanced oleylammonium–oleate salt complex, which would also be the source of the minor features near 1407 and 1538 cm^{-1} from oleate $\nu(COO^-)$ symmetric and asymmetric stretching modes, respectively. These major differences in the FTIR spectra provide further evidence for successful generation of $PbBr_2$ NCs via CsBr salt extraction from $CsPbBr_3$ NCs.

In the rest of this work, we detail our key finding that the $PbBr_2$ NCs derived from $CsPbBr_3$ NCs react readily with solutions of ABr salt (A = MA^+, FA^+, Cs^+) in glacial acetic acid (CH_3COOH) to form an array of new low-dimensional structures within the confines of the NC framework (Scheme 1). These dilute 0.01 M ABr salt solutions presumably exist as A′X′, where A′ = A or H^+ and X′ = Br^- or CH_3COO^-, and provide a source of either MA^+, FA^+, Cs^+, or H^+ cations as well as both Br^- and CH_3COO^- anions to the $PbBr_2$ NCs. Depending on the volume fractions of the $PbBr_2$ NC solution (ν_{NC} = 0.1–0.4) and concentration of A′X′ salt solution, we find that the process yields $A'_2A_{n-1}Pb_nBr_{3n-1}X'_2$ NCs where n = 1, 2, 3, ...∞, which corresponds to the number of $PbBr_2$ layers comprising discrete 2DN sheets making up the NC (Figure 2).

There is a large class of related bulk 2D Ruddlesden–Popper-type perovskites, for example, $(C_6H_5C_2H_4NH_3)_2PbBr_4$[39] and $Cs_2[C(NH_2)_3]Pb_2Br_7$.[40] Such bulk 2D phases have been the subject of intense interest over the last several years, and we point the reader to recent

DOI: 10.1021/acs.jpcc.8b01164
J. Phys. Chem. C XXXX, XXX, XXX–XXX

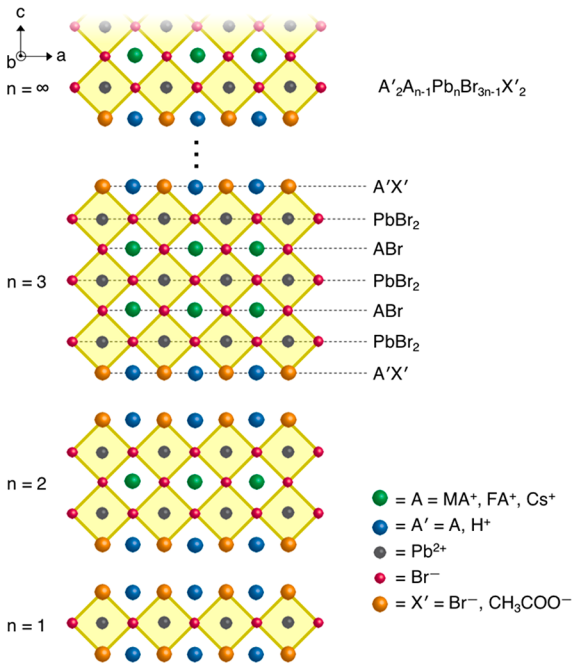

Figure 2. Diagram of the 2DN layered $A'_2A_{n-1}Pb_nBr_{3n-1}X'_2$ compounds present within the NC framework observed in this work.

reviews.[41−44] Briefly, formation of low-dimensional perovskite networks is achieved by slicing the three-dimensional AMX_3 crystal along specific lattice planes. Slicing along the (001) plane results in the 2D structure type $A'_2A_{n-1}M_nX_{3n+1}$, (X = Cl^-, Br^-, I^-) where n corresponds to the number of MX_2 layers in the structure. An example compound for n = 1 is $(C_6H_5C_2H_4NH_3)_2PbBr_4$ and n = 2 for $Cs_2[C(NH_2)_3]Pb_2Br_7$. A molecular dication may also span the two A′-sites across adjacent MX_2 layers. For example, combining $PbBr_2$ with 2-(aminomethyl)pyridine (2-AMP) has resulted in an n = 1 2DN sheet structure consisting of $(H_2$2-AMP$)PbBr_4$ characterized by an excitonic absorption feature at 2.87 eV.[45] In all cases, the prior reports of the synthesis of bulk 2D perovskites involve adding (1) the desired salt(s) to B metal precursor solutions; (2) a large-for-small cation exchange by adding AX salt to the preformed bulk AMX_3 structure; or (3) a neutral molecule that intercalates into and expands the A cation layer. The structural and optical properties of these phase-pure, bulk 2D perovskites in single crystal and film form have been explored extensively in both decades old[46−48] and recent studies[36,41−44] and provide valuable background for the present work.

We perform a series of conversion experiments using A′X′ salt solutions (A = MA^+), in which the total reaction solution volume is held constant. The volume fraction of the $PbBr_2$ NC solution as well as the concentration of (MA)Br ($C_{(MA)Br}$) and acetic acid (C_{HOAc}) are varied. The critical nature of the composition of these solutions is evident from photographs of the NC solutions under UV illumination (Figure 3a−c). The parent $CsPbBr_3$ and $PbBr_2$ NCs are shown for comparison (Figure 3a,b), which exhibit bright green and no emission, respectively (as shown in Figure 1a). Conditions are varied to achieve $A'_2A_{n-1}Pb_nBr_{3n-1}X'_2$ NCs with blue emission, which corresponds to 2DN layered structures (Figure 3c, leftmost cuvette) and the homogeneous product (MA)$PbBr_3$ (Figure 3c, rightmost cuvette, n = ∞). This homogeneous product results from an effective A-site cation exchange where MA^+ is substituted for Cs^+ from the parent $CsPbBr_3$ NCs, which is

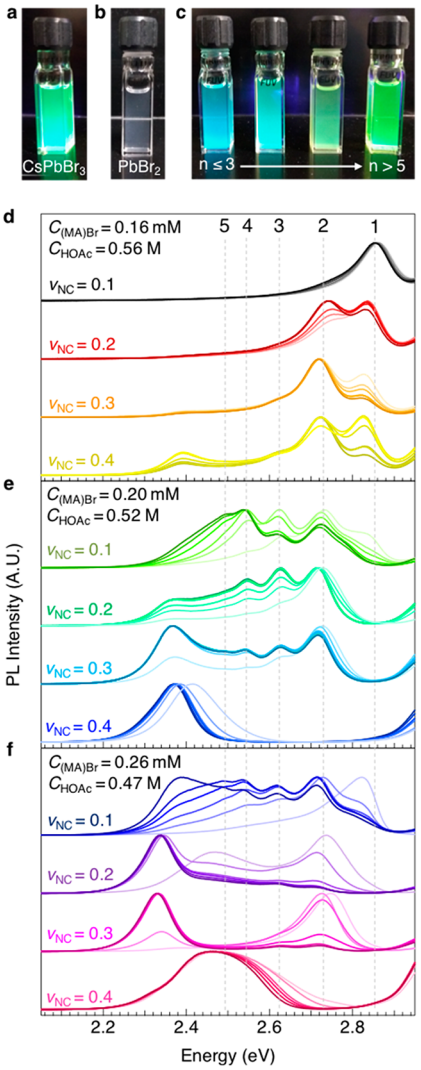

Figure 3. PL evolution of $A'_2A_{n-1}Pb_nBr_{3n-1}X'_2$ NCs. Photographs of solutions of (a) the parent $CsPbBr_3$, (b) salt-extracted $PbBr_2$ NCs, and (c) $A'_2A_{n-1}Pb_nBr_{3n-1}X'_2$ NCs (A = MA^+) with n increasing from left to right. (d−f) Time-resolved PL spectra of $A'_2A_{n-1}Pb_nBr_{3n-1}X'_2$ NCs (A = MA^+) at varying $PbBr_2$ NC solution volume fractions (v_{NC}) and (MA)Br concentration ($C_{(MA)Br}$) and HOAc concentration (C_{HOAc}) values. Each set of time-evolution spectra are normalized in intensity and offset vertically for clarity. The light-colored spectrum in each set is the initial spectrum, and the darkest color is the final spectrum. The spectra are taken from t = 0 to t = 180 min in 30 min intervals. Gray dashed vertical lines indicate n values.

enabled by the charge-balancing Br^- anion also undergoing extraction and reinsertion with the cations.

Close examination of Figure 3d−f shows the dynamic evolution of the PL spectra that give rise to the blue-shifted emission from the photographs in Figure 3c. A low $PbBr_2$ NC solution total volume fraction (v_{NC} = 0.1), a low (MA)Br salt concentration ($C_{(MA)Br}$ = 0.16 M) and a high acetic acid concentration (C_{HOAc} = 0.56 M) generates a $A'_2A_{n-1}Pb_nBr_{3n-1}X'_2$ NC solution with a single high-energy emission peak at 2.85 eV that does not appreciably evolve over the course of 3 h (black spectra, Figure 3d). When the volume fraction of $PbBr_2$ NC solution is increased (v_{NC} = 0.2−0.4), a variety of PL peaks are observed, and the peaks evolve with time. Time-resolved spectra taken at t = 0 and every 30 min following salt solution addition reveal that it takes ∼3 h to

DOI: 10.1021/acs.jpcc.8b01164
J. Phys. Chem. C XXXX, XXX, XXX−XXX

reach an equilibrium $A'_2A_{n-1}Pb_nBr_{3n-1}X'_2$ NC composition at ambient temperature (red, orange, and yellow spectra, Figure 3d). Several interesting features are observed upon close inspection of the time-resolved PL spectra. Immediately after $PbBr_2$ NCs are added to acetic acid-diluted A′X′ salt solution, for all $v_{NC} > 0.1$, additional peaks emerge at lower energies relative to the highest energy peak found in the $v_{NC} = 0.1$ sample (2.85 eV). The same trend is observed at lower concentrations of acetic acid and higher concentrations of (MA)Br salt: $C_{HOAc} = 0.52$ M and $C_{(MA)Br} = 0.20$ M (Figure 3e) and $C_{HOAc} = 0.47$ and $C_{(MA)Br} = 0.26$ M (Figure 3f). Under these lower acetic acid and higher (MA)Br salt concentration conditions, even more complex temporal evolution generally is observed, with initial high-energy peaks evolving into lower-energy peaks with time. The exception is the "Goldilocks" conditions where a balance of the $PbBr_2$ volume fraction ($v_{NC} = 0.4$) along with moderate concentrations of (MA)Br salt ($C_{(MA)Br} = 0.20$ M) and acetic acid ($C_{HOAc} = 0.56$ M) gives rise to a homogeneous product with the lowest peak emission energy at 2.39 eV (blue spectra, Figure 3f).

To account for these PL results, we posit that the observed emission peaks result from different n values of $A'_2A_{n-1}Pb_nBr_{3n-1}X'_2$ 2DN sheets within the NCs. Such 2DN layered perovskites with similar emission spectra have been observed previously by several groups but not in nanocrystalline form. In 2015, Urban and co-workers showed that $(MA)PbBr_3$ nanoplatelets are obtained with PL energies from 2.90−2.39 eV depending on the octylammonium bromide concentration after adding octylammonium bromide salt to (MA)Br and $PbBr_2$ in DMF solution.[49] Later that year, Alivisatos and co-workers reported that $CsPbBr_3$ nanoplatelets are generated by reducing the temperature of the conventional 140−200 °C $CsPbBr_3$ NC synthesis to 90−130 °C and isolating the resulting nanoplatelets using ethyl acetate or methyl ethyl ketone (low water content) antisolvents.[50] Fractions containing both $n = 1$, 2 and $n = 3$, 4, 5 layers were obtained, and emission energies were resolved for all samples: 3.06 eV ($n = 1$), 2.85 eV ($n = 2$), 2.68 eV ($n = 3$), 2.60 eV ($n = 4$), and 2.54 eV ($n = 5$). Shortly thereafter, Manna and co-workers showed that by adding various amounts of HBr, the $CsPbBr_3$ NC synthesis also generated $CsPbBr_3$ nanoplatelets with emission energies from 2.83−2.70 eV ($n = 3$−5), and DFT results in the same paper suggested that PL should be observed within 2.84−2.36 eV for $n = 1\cdots\infty$.[51] Related work by the same group showed that $PbBr_2$ could be added to $CsPbBr_3$ NCs to generate Cs_4PbBr_6 wide bandgap NCs (emission 3.99 eV).[15] Finally, Oron, Kazes, and co-workers recently reported that these Cs_4PbBr_6 insulator NCs can be reversibly transformed into $CsPbBr_3$ nanoplatelets driven by the oleylamine/oleic acid surfactant ligand ratio.[51] Several assignments were made by comparing their PL spectra to the results from Manna and co-workers, though it is unclear whether the experimental or theoretical data were used.

In our work, the presence of acetic acid as the solvent in our ABr salt solutions (A = MA^+, FA^+, Cs^+) results in a salt formulation that is best described as A′X′ where A′ = A or H^+ and X′ = Br^- or CH_3COO^-. Based on this chemistry as well as prior work on bulk 2DN structures and isolated 2DN nanoplatelets, the dynamic evolution in the emission spectra in Figure 3d−f is rationalized. First, these PL data provide convincing evidence that lower n values in $A'_2A_{n-1}Pb_nBr_{3n-1}X'_2$ 2DN sheets occur under higher C_{HOAc} and lower $C_{(MA)Br}/v_{NC}$ conditions. Second, a homogeneous product is formed under certain conditions (Figure 3e, blue spectra) that exhibits the same size and size dispersity as the parent $CsPbBr_3$ NCs (vide infra). This homogeneous product is assigned to the fully cation-exchanged $(MA)PbBr_3$ NC, which suggests that the other products in solution giving rise to higher-energy peaks at earlier times also retain the size and size dispersity of the parent NCs. The peak evolution also suggests the 2DN sheets are not isolated but are derived from the monolithic $PbBr_2$ NC precursor.

Therefore, under most conditions, we proposed that acetate anions are the initial X′ species that bind to and separate some of the haloplumbate(II) layers in $PbBr_2$ NCs and/or terminate the surface of $A'_2A_{n-1}Pb_nBr_{3n-1}X'_2$ NCs (orange balls, Figure 2). Acetate incorporation appears to be preferred kinetically, since stronger blue-shifted PL peaks are observed at early times in the time-resolved PL spectra in Figure 3d−f, whereas bromide incorporation into the NC lattice is preferred thermodynamically based on PL red-shifts toward lower energy 2DN and eventually 3D structures at later times under low C_{HOAc} and high v_{NC}. This kinetic preference for acetate incorporation is likely due to the significantly higher concentration of acetate relative to bromide (≤0.26 mM ABr salt solutions in glacial acetic acid). Since evolution toward higher n values occurs over time, we conclude that the Pb(II)−Br bond is slightly more favorable thermodynamically than the bidentate $Pb(II)-OOCCH_3$ bond. Thus, Le Chatelier's principle ultimately governs the structure obtained at equilibrium. At high C_{HOAc} relative to the number of $PbBr_2$ NCs (low v_{NC}), the equilibrium shifts sufficiently toward complete conversion to a single-layer $n = 1$ $A'_2PbBr_2X'_2$ phase. Alternatively, decreasing C_{HOAc} shifts the equilibrium toward the all-bromide 3D $APbBr_3$ NC. Since the surface structure of NCs is still dominated by the A′X′ salt and/or surfactant ions (see FTIR data, Figure 1g), we prefer the $A'_2A_{n-1}Pb_nBr_{3n-1}X'_2$ formula even for these homogeneous 3D NCs.

Finally, we note that the presence of protons also may aid acetate versus bromide incorporation at early times (pK_a 4.76 for CH_3COOH vs −9 for HBr in aqueous solution). The physical parameters affecting the degree of acetate incorporation is likely highly complex, since evolution does not progress through isosbestic points in the time-resolved PL spectra. However, acetate does appear to preferentially incorporate into the $A'_2A_{n-1}Pb_nBr_{3n-1}X'_2$ NC along single planes, since unique emission peaks (corresponding to discrete n values) are observed in the time-resolved PL spectra. By comparison to prior nanoplatelet data, we propose the PL peaks observed at 2.85, 2.73, 2.62, 2.54, and 2.49 eV result from $n = 1$, 2, 3, 4, and 5 2DN MHP layers, respectively. As summarized in Table S1, these PL peak energies for the samples described here are very close but slightly red-shifted from those observed for octylammonium ligands on the related "$(MA)PbBr_3$" $n = 1$−5 nanoplatelets. In particular, the largest difference of 50 meV is observed for the $n = 1$ sample in previous work[49] where no MA is present and the octylammonium ligands are in the A′-site terminating a single layer of corner-sharing $PbBr_6$ octahedra. We posit that these long chain octylammonium[50] organic surfactants separating the sheets provide electronic isolation between individual nanoplatelets, whereas smaller X′ molecules (e.g., CH_3COO^-) as well as A′ cations (H^+ or MA^+) in 2DN structures within the $A'_2A_{n-1}Pb_nBr_{3n-1}X'_2$ NCs described here provide some degree of electronic coupling between adjacent 2DN sheets. A related red-shift has been observed in PbSe NC films upon exchanging

DOI: 10.1021/acs.jpcc.8b01164
J. Phys. Chem. C XXXX, XXX, XXX−XXX

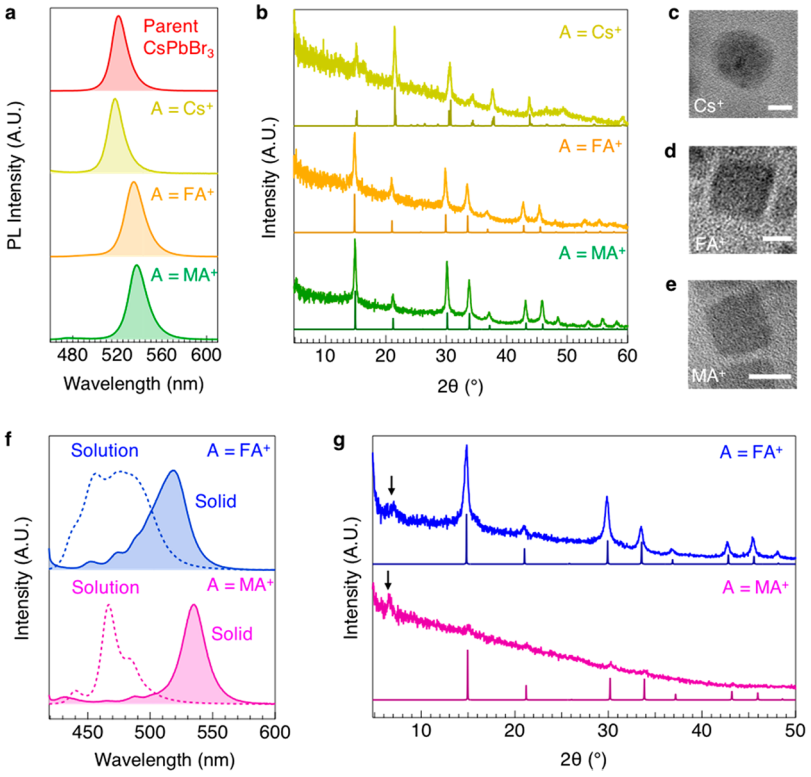

Figure 4. Characterization of $A'_2A_{n-1}Pb_nBr_{3n-1}X'_2$ NCs. (a) PL spectra of the parent $CsPbBr_3$ NCs (red) and $A'_2A_{n-1}Pb_nBr_{3n-1}X'_2$ NCs for the three different cations (A = Cs^+, FA^+, MA^+) investigated in this study. ν_{NC} = 0.4, C_{ABr} = 0.20 mM, and $_{HOAc}$= 0.52 M for each spectrum. Spectra are normalized and offset for clarity. (b) XRD patterns of $A'_2A_{n-1}Pb_nBr_{3n-1}X'_2$ NCs synthesized with A = Cs^+ (yellow), FA^+ (orange), and MA^+ (green). Simulated powder diffraction patterns of the corresponding crystals are shown below each pattern. Patterns are normalized and offset for clarity. (c–e) TEM images of an individual NC converted with (c) CsBr, (d) (FA)Br, and (e) (MA)Br. Scale bars are 5 nm. (f) PL spectra of $A'_2A_{n-1}Pb_nBr_{3n-1}X'_2$, in which A = FA^+ (blue) or A = MA^+ (purple) in solution (dashed) and after centrifugation to isolate NCs (solid). (g) XRD patterns of $A'_2A_{n-1}Pb_nBr_{3n-1}X'_2$ NCs synthesized with A = FA^+ (blue) and MA^+ (magenta) that correspond to the solid PL spectra shown in (f). Simulated powder diffraction patterns of the corresponding crystals are shown below each pattern. Patterns are normalized and offset for clarity. Arrows in XRD patterns highlight the low angle peak that cannot be attributed to $APbBr_3$.

the native oleate ligands for methoxide owing to the decreased interparticle spacing (and greater wave function overlap) with methoxide.[52] Another likely influence in the observed red-shift for our n = 1–5 MA^+-based $A'_2A_{n-1}Pb_nBr_{3n-1}X'_2$ NCs is the well-known bathochromic shift[53] where the close spacing of the 2DN sheets (enabled by short acetate molecules) gives a more solid-state-like dielectric environment than the organic ligands surrounding isolated nanoplatelets.

We find that homogeneous samples are only obtained with a specific $PbBr_2$ volume fraction (ν_{NC} = 0.4) as well as specific salt ($C_{(MA)Br}$ = 0.20 mM) and acetic acid (C_{HOAc} = 0.52 M) concentrations. The required conditions for complete conversion to a homogeneous 3D $A'_2A_{n-1}Pb_nBr_{3n-1}X'_2$ NC product should be monitored by simply titrating A′X′ salt solutions in acetic acid into each $PbBr_2$ NC solution under different surfactant ligand concentrations. An example of this titration experiment is depicted in Supplementary Movie 1. This step is necessary, since the absolute surfactant ligand concentration is critical and difficult to control from batch to batch of $PbBr_2$ NCs. Excess surfactant ligand is needed to stabilize solutions of NCs. If there is too much surfactant ligand, then $PbBr_2$ NCs do not convert to $A'_2A_{n-1}Pb_nBr_{3n-1}X'_2$ NCs after salt solution addition, and instead, no color change of the solution is observed. Conversely, if the surfactant ligand concentration is too low, the NCs agglomerate and precipitate from solution. Thus, minor adjustments to added surfactant ligand concentrations may be necessary for each $PbBr_2$ batch. In practice, we find that the required amount of additional OAm and OA can vary between 0.01–0.025 mL each per 2.5 mL of total solution volume (see Experimental Methods).

Figure 4a shows the PL spectra of $A'_2A_{n-1}Pb_nBr_{3n-1}X'_2$ (A = MA^+, FA^+, Cs^+) NCs obtained after CsBr salt extraction from $CsPbBr_3$ NCs and addition of A′X′ salt solutions to reach a homogeneous product with emission comparable to the parent $CsPbBr_3$ NCs (2.39 eV for A = Cs^+; 2.32 eV for A = FA^+; 2.31 eV for A = MA^+) with fwhm values remaining at 82 meV in all cases. These data show that the overall cation exchange process retains the size and size distribution of the parent $CsPbBr_3$ NCs. This result provides strong evidence that the $PbBr_2$ NC intermediates are derived directly from salt extraction from the parent NCs and reinsertion into $PbBr_2$ NCs without significant loss or gain of Pb^{2+} cations. TEM of isolated, homogeneous 3D NCs after conversion further suggests that the intermediates observed in the time-resolved PL experiments are derived from salt extraction and reinsertion within monolithic NCs. Compared to the parent NCs (Figure 1b), NCs converted with CsBr, (MA)Br, and (FA)Br show a similar dimensions of 10 nm (Figures 4c–e and S1). XRD patterns of the isolated NCs are consistent with the formation of $APbBr_3$ NCs with cubic (*Pnma*) crystal structures (Figure 4f). The peak broadness in the converted NCs is similar to that of the parent $CsPbBr_3$ NCs, and characteristic peaks for each sample matches its simulated pattern (Figure 4f). FTIR analysis of the 2DN $A'_2A_{n-1}Pb_nBr_{3n-1}X'_2$ NCs shows characteristic signatures of the

DOI: 10.1021/acs.jpcc.8b01164
J. Phys. Chem. C XXXX, XXX, XXX–XXX

A-site cations used during conversion and further validates conversion of $PbBr_2$ NCs (Figure S2).

The low formation energies of MHPs make purification and isolation challenging, which has been pointed out by many research groups.[34,51] Our efforts to isolate both 3D $APbBr_3$ and layered 2DN $A'_2A_{n-1}Pb_nBr_{3n-1}X'_2$ NCs were challenging. Isolation of 2DN compounds was unsuccessful using a variety of conditions that appear to fundamentally change the nature of the NCs. For example, the oleylamine and oleic acid in acetone solution used to precipitate the parent $CsPbBr_3$ NCs is ineffective at precipitating 2DN $A'_2A_{n-1}Pb_nBr_{3n-1}X'_2$ NCs. Similarly, the antisolvent methyl acetate, previously used to isolate $CsPbI_3$ NCs,[34] also results in a transparent, colorless solution rather than precipitated NCs. Instead, we find addition of extra A′X′ solution (~100 μL to 2.5 mL of total solution volume) leads to flocculation. Subsequent centrifugation allows isolation of a solid product that exhibits a red-shifted emission spectrum compared to emission in solution (Figures S3 and 4f), which indicates that the $A'_2A_{n-1}Pb_nBr_{3n-1}X'_2$ NCs observed in solution may need the acetic acid environment to maintain the layered structures and are extremely difficult to isolate. Still, the PL spectra of isolated NCs in Figure 4f maintain a some degree of high-energy emission peaks that correspond to layered 2DN compounds. Notably, the XRD patterns of the corresponding isolated NCs exhibit a low-angle reflection between $2\theta = 6$ and 7° (Figure 4g, black arrows). These low-angle reflections correspond to a lattice spacing between 6.2 and 6.8 Å that is inconsistent with a 3D $(MA)PbBr_3$ structure and are characteristic of the (002) reflection from a 2DN material structure where the 6.2 Å spacing reflects the distance between layered and stacked perovskite sheets, separated by acetate anions at the X′ position in the external haloplumbate-(II) layers of each sheet (orange balls, Figure 2).

CONCLUSIONS

In this work, we demonstrate tuned emission from an array of $A'_2A_{n-1}Pb_nBr_{3n-1}X'_2$ NCs with varying A′, X′, and *n*. The $A'_2A_{n-1}Pb_nBr_{3n-1}X'_2$ NCs are produced by extracting CsBr from $CsPbBr_3$ to yield $PbBr_2$ NCs followed by AX′ salt reinsertion, formed by dissolving ABr in glacial acetic acid, into the $PbBr_2$ structure. This process represents a versatile new method for producing NCs with different A-site cations and tunable emission, which is dictated by both solution kinetics and thermodynamics. It is an interesting example where the unique solution environment for producing new materials is not accessible using conventional methods. This method of salt extraction and reinsertion opens up possibilities of making in situ formation measurement on 2DN perovskites as well as 3D perovskite NCs and films that could be crucial to understanding synthesis and stability.

ASSOCIATED CONTENT

Supporting Information

The Supporting Information is available free of charge on the ACS Publications website at DOI: 10.1021/acs.jpcc.8b01164.

Table of emission data as a function of 2DN layer thickness from this and prior works; TEM of arrays of converted NCs; FTIR spectra and analysis of $A'_2A_{n-1}Pb_nBr_{3n-1}X'_2$NCs; PL spectra of solution and isolated NCs (PDF)

Movie showing titration of $(MA)X'$ solution into $PbBr_2$ NC solution (MPG)

AUTHOR INFORMATION

Corresponding Authors

*E-mail: lance.wheeler@nrel.gov (L.M.W.)

*E-mail: nathan.neale@nrel.gov (N.R.N.)

ORCID

Lance M. Wheeler: 0000-0002-1685-8242

Matthew P. Hautzinger: 0000-0002-4764-3076

Nathan R. Neale: 0000-0001-5654-1664

Present Address

[‖]Department of Chemistry, University of Wisconsin-Madison, 1101 University Avenue, Madison, Wisconsin 53706, United States (M.P.H.)

Notes

The authors declare no competing financial interest.

ACKNOWLEDGMENTS

Project conception, data collection and interpretation were supported by the U.S. Department of Energy, Office of Science, Office of Basic Energy Sciences, Division of Chemical Sciences, Geosciences, and Biosciences, Solar Photochemistry Program under contract number DE-AC36-08GO28308 with the Alliance for Sustainable Energy, LLC, the Manager and Operator of the National Renewable Energy Laboratory (L.M.W, N.C.A., and N.R.N.). T.B. and M.P.H. acknowledge support for concentration-dependent studies by the U.S. Department of Energy, Office of Science, Office of Workforce Development for Teachers and Scientists (WDTS) under the Science Undergraduate Laboratory Internships (SULI) program at NREL.

REFERENCES

(1) Zhang, W.; Eperon, G. E.; Snaith, H. J. Metal Halide Perovskites for Energy Applications. *Nat. Energy* **2016**, *1*, 16048.

(2) Christians, J. A.; Schulz, P.; Tinkham, J. S.; Schloemer, T. H.; Harvey, S. P.; Tremolet de Villers, B. J.; Sellinger, A.; Berry, J. J.; Luther, J. M. Tailored Interfaces of Unencapsulated Perovskite Solar Cells for > 1,000 h Operational Stability. *Nat. Energy* **2018**, *3*, 68−74.

(3) Yang, W. S.; Park, B.-W.; Jung, E. H.; Jeon, N. J.; Kim, Y. C.; Lee, D. U.; Shin, S. S.; Seo, J.; Kim, E. K.; Noh, J. H.; et al. Iodide Management in Formamidinium-Lead-Halide−Based Perovskite Layers for Efficient Solar Cells. *Science* **2017**, *356*, 1376−1379.

(4) Sanehira, E. M.; Marshall, A. R.; Christians, J. A.; Harvey, S. P.; Ciesielski, P. N.; Wheeler, L. M.; Schulz, P.; Lin, L. Y.; Beard, M. C.; Luther, J. M. Enhanced Mobility $CsPbI_3$ Quantum Dot Arrays for Record-Efficiency, High-Voltage Photovoltaic Cells. *Sci. Adv.* **2017**, *3*, eaao4204.

(5) Yakunin, S.; Protesescu, L.; Krieg, F.; Bodnarchuk, M. I.; Nedelcu, G.; Humer, M.; De Luca, G.; Fiebig, M.; Heiss, W.; Kovalenko, M. V. Low-Threshold Amplified Spontaneous Emission and Lasing From Colloidal Nanocrystals of Caesium Lead Halide Perovskites. *Nat. Commun.* **2015**, *6*, 8056.

(6) Becker, M. A.; Vaxenburg, R.; Nedelcu, G.; Sercel, P. C.; Shabaev, A.; Mehl, M. J.; Michopoulos, J. G.; Lambrakos, S. G.; Bernstein, N.; Lyons, J. L.; et al. Bright Triplet Excitons in Caesium Lead Halide Perovskites. *Nature* **2018**, *553*, 189−193.

(7) Bae, W. K.; Padilha, L. A.; Park, Y.-S.; McDaniel, H.; Robel, I.; Pietryga, J. M.; Klimov, V. I. Controlled Alloying of the Core−Shell Interface in CdSe/CdS Quantum Dots for Suppression of Auger Recombination. *ACS Nano* **2013**, *7*, 3411−3419.

(8) Liu, F.; Zhang, Y.; Ding, C.; Kobayashi, S.; Izuishi, T.; Nakazawa, N.; Toyoda, T.; Ohta, T.; Hayase, S.; Minemoto, T.; Yoshino, K.; Dai, S.; Shen, Q. Highly Luminescent Phase-Stable CsPbI 3Perovskite Quantum Dots Achieving Near 100% Absolute Photoluminescence Quantum Yield. *ACS Nano* **2017**, *11*, 10373−10383.

DOI: 10.1021/acs.jpcc.8b01164
J. Phys. Chem. C XXXX, XXX, XXX−XXX

(9) Koscher, B. A.; Swabeck, J. K.; Bronstein, N. D.; Alivisatos, A. P. Essentially Trap-Free $CsPbBr_3$ Colloidal Nanocrystals by Postsynthetic Thiocyanate Surface Treatment. *J. Am. Chem. Soc.* **2017**, *139*, 6566−6569.
(10) Di Stasio, F.; Christodoulou, S.; Huo, N.; Konstantatos, G. Near-Unity Photoluminescence Quantum Yield in CsPbBr 3Nanocrystal Solid-State Films via Postsynthesis Treatment with Lead Bromide. *Chem. Mater.* **2017**, *29*, 7663−7667.
(11) Swarnkar, A.; Marshall, A. R.; Sanehira, E. M.; Chernomordik, B. D.; Moore, D. T.; Christians, J. A.; Chakrabarti, T.; Luther, J. M. Quantum Dot-Induced Phase Stabilization of A-CsPbI3 Perovskite for High-Efficiency Photovoltaics. *Science* **2016**, *354*, 92−95.
(12) Nenon, D. P.; Christians, J. A.; Wheeler, L. M.; Blackburn, J. L.; Sanehira, E. M.; Dou, B.; Olsen, M. L.; Zhu, K.; Berry, J. J.; Luther, J. M. Structural and Chemical Evolution of Methylammonium Lead Halide Perovskites During Thermal Processing From Solution. *Energy Environ. Sci.* **2016**, *9*, 2072−2082.
(13) Wheeler, L. M.; Moore, D. T.; Miller, E. M.; Blackburn, J. L.; Neale, N. R.; Stanton, N. J.; Ihly, R.; Tenent, R. C. Switchable Photovoltaic Windows Enabled by Reversible Photothermal Complex Dissociation From Methylammonium Lead Iodide. *Nat. Commun.* **2017**, *8*, 1722.
(14) Nedelcu, G.; Protesescu, L.; Yakunin, S.; Bodnarchuk, M. I.; Grotevent, M. J.; Kovalenko, M. V. Fast Anion-Exchange in Highly Luminescent Nanocrystals of Cesium Lead Halide Perovskites ($CsPbX_3$, X = Cl, Br, I). *Nano Lett.* **2015**, *15*, 5635−5640.
(15) Akkerman, Q. A.; D'Innocenzo, V.; Accornero, S.; Scarpellini, A.; petrozza, A.; Prato, M.; Manna, L. Tuning the Optical Properties of Cesium Lead Halide Perovskite Nanocrystals by Anion Exchange Reactions. *J. Am. Chem. Soc.* **2015**, *137*, 10276−10281.
(16) Mefford, J. T.; Hardin, W. G.; Dai, S.; Johnston, K. P.; Stevenson, K. J. Anion Charge Storage Through Oxygen Intercalation in $LaMnO_3$ Perovskite Pseudocapacitor Electrodes. *Nat. Mater.* **2014**, *13*, 726−732.
(17) Eperon, G. E.; Ginger, D. S. B-Site Metal Cation Exchange in Halide Perovskites. *ACS Energy Lett.* **2017**, *2*, 1190−1196.
(18) van der Stam, W.; Geuchies, J. J.; Altantzis, T.; van den Bos, K. H. W.; Meeldijk, J. D.; Van Aert, S.; Bals, S.; Vanmaekelbergh, D.; de Mello Donega, C. Highly Emissive Divalent-Ion-Doped Colloidal $CsPb_{1-x}M_xBr_3$ Perovskite Nanocrystals Through Cation Exchange. *J. Am. Chem. Soc.* **2017**, *139*, 4087−4097.
(19) Gao, D.; Qiao, B.; Xu, Z.; Song, D.; Song, P.; Liang, Z.; Shen, Z.; Cao, J.; Zhang, J.; Zhao, S. Postsynthetic, Reversible Cation Exchange Between Pb^{2+} and Mn^{2+} in Cesium Lead Chloride Perovskite Nanocrystals. *J. Phys. Chem. C* **2017**, *121*, 20387−20395.
(20) Li, Z.; Yang, M.; Park, J.-S.; Wei, S.-H.; Berry, J. J.; Zhu, K. Stabilizing Perovskite Structures by Tuning Tolerance Factor: Formation of Formamidinium and Cesium Lead Iodide Solid-State Alloys. *Chem. Mater.* **2016**, *28*, 284−292.
(21) Eperon, G. E.; Beck, C. E.; Snaith, H. J. Cation Exchange for Thin Film Lead Iodide Perovskite Interconversion. *Mater. Horiz.* **2016**, *3*, 63−71.
(22) Hills-Kimball, K.; Nagaoka, Y.; Cao, C.; Chaykovsky, E.; Chen, O. Synthesis of Formamidinium Lead Halide Perovskite Nanocrystals Through Solid-Liquid-Solid Cation Exchange. *J. Mater. Chem. C* **2017**, *5*, 5680−5684.
(23) Tsunoda, Y.; Sugimoto, W.; Sugahara, Y. Intercalation Behavior of N-Alkylamines Into a Protonated Form of a Layered Perovskite Derived From Aurivillius Phase $Bi_2SrTa_2O_9$. *Chem. Mater.* **2003**, *15*, 632−635.
(24) Mitzi, D. B.; Chondroudis, K.; Kagan, C. R. Organic-Inorganic Electronics. *IBM J. Res. Dev.* **2001**, *45*, 29−45.
(25) Quan, L. N.; Yuan, M.; Comin, R.; Voznyy, O.; Beauregard, E. M.; Hoogland, S.; Buin, A.; Kirmani, A. R.; Zhao, K.; Amassian, A.; Kim, D. H.; Sargent, E. H. Ligand-Stabilized Reduced-Dimensionality Perovskites. *J. Am. Chem. Soc.* **2016**, *138*, 2649−2655.
(26) Mitzi, D. B.; Wang, S.; Feild, C. A.; Chess, C. A.; Guloy, A. M. Conducting Layered Organic-Inorganic Halides Containing-Oriented Perovskite Sheets. *Science* **1995**, *267*, 1473−1476.
(27) Cheng, Z.; Lin, J. Layered Organic−Inorganic Hybrid Perovskites: Structure, Optical Properties, Film Preparation, Patterning and Templating Engineering. *CrystEngComm* **2010**, *12*, 2646−2662.
(28) Liu, Z.; Bekenstein, Y.; Ye, X.; Nguyen, S. C.; Swabeck, J.; Zhang, D.; Lee, S.-T.; Yang, P.; Ma, W.; Alivisatos, A. P. Ligand Mediated Transformation of Cesium Lead Bromide Perovskite Nanocrystals to Lead Depleted Cs_4PbBr_6 Nanocrystals. *J. Am. Chem. Soc.* **2017**, *139*, 5309−5312.
(29) Palazon, F.; Urso, C.; De Trizio, L.; Akkerman, Q.; Marras, S.; Locardi, F.; Nelli, I.; Ferretti, M.; Prato, M.; Manna, L. Postsynthesis Transformation of Insulating Cs_4PbBr_6 Nanocrystals Into Bright Perovskite $CsPbBr_3$ through Physical and Chemical Extraction of CsBr. *ACS Energy Lett.* **2017**, *2*, 2445−2448.
(30) Hassan, Y.; Song, Y.; Pensack, R. D.; Abdelrahman, A. I.; Kobayashi, Y.; Winnik, M. A.; Scholes, G. D. Structure-Tuned Lead Halide Perovskite Nanocrystals. *Adv. Mater.* **2016**, *28*, 566−573.
(31) Balakrishnan, S. K.; Kamat, P. V. Ligand Assisted Transformation of Cubic $CsPbBr_3$ Nanocrystals Into Two-Dimensional $CsPb_2Br_5$ Nanosheets. *Chem. Mater.* **2018**, *30*, 74−78.
(32) Shamsi, J.; Dang, Z.; Ijaz, P.; Abdelhady, A. L.; Bertoni, G.; Moreels, I.; Manna, L. Colloidal CsX (X = Cl, Br, I) Nanocrystals and Their Transformation to $CsPbX_3$ Nanocrystals by Cation Exchange. *Chem. Mater.* **2018**, *30*, 79−83.
(33) Udayabhaskararao, T.; Kazes, M.; Houben, L.; Lin, H.; Oron, D. Nucleation, Growth, and Structural Transformations of Perovskite Nanocrystals. *Chem. Mater.* **2017**, *29*, 1302−1308.
(34) Protesescu, L.; Yakunin, S.; Bodnarchuk, M. I.; Krieg, F.; Caputo, R.; Hendon, C. H.; Yang, R. X.; Walsh, A.; Kovalenko, M. V. Nanocrystals of Cesium Lead Halide Perovskites ($CsPbX_3$, X = Cl, Br, and I): Novel Optoelectronic Materials Showing Bright Emission with Wide Color Gamut. *Nano Lett.* **2015**, *15*, 3692−3696.
(35) Stoumpos, C. C.; Malliakas, C. D.; Peters, J. A.; Liu, Z.; Sebastian, M.; Im, J.; Chasapis, T. C.; Wibowo, A. C.; Chung, D. Y.; Freeman, A. J.; Wessels, B. W.; Kanatzidis, M. G. Crystal Growth of the Perovskite Semiconductor $CsPbBr_3$: a New Material for High-Energy Radiation Detection. *Cryst. Growth Des.* **2013**, *13*, 2722−2727.
(36) Nieuwenkamp, W.; Bijvoet, J. M. Die Kristallstruktur Von Bleibromid $PbBr_2$. *Z. Kristallogr. - Cryst. Mater.* **1933**, *84*, 49.
(37) De Roo, J.; Ibáñez, M.; Geiregat, P.; Nedelcu, G.; Walravens, W.; Maes, J.; Martins, J. C.; Van Driessche, I.; Kovalenko, M. V.; Hens, Z. Highly Dynamic Ligand Binding and Light Absorption Coefficient of Cesium Lead Bromide Perovskite Nanocrystals. *ACS Nano* **2016**, *10*, 2071−2081.
(38) Wheeler, L. M.; Nichols, A. W.; Chernomordik, B. D.; Anderson, N. C.; Beard, M. C.; Neale, N. R. All-Inorganic Germanium Nanocrystal Films by Cationic Ligand Exchange. *Nano Lett.* **2016**, *16*, 1949−1954.
(39) Mitzi, D. B. Synthesis, Structure, and Properties of Organic-Inorganic Perovskites and Related Materials. *Prog. Inorg. Chem.* **2007**, *48*, 1−121.
(40) Nazarenko, O.; Kotyrba, M. R.; Wörle, M.; Cuervo-Reyes, E.; Yakunin, S.; Kovalenko, M. V. Luminescent and Photoconductive Layered Lead Halide Perovskite Compounds Comprising Mixtures of Cesium and Guanidinium Cations. *Inorg. Chem.* **2017**, *56*, 11552−11564.
(41) Saparov, B.; Mitzi, D. B. Organic−Inorganic Perovskites: Structural Versatility for Functional Materials Design. *Chem. Rev.* **2016**, *116*, 4558−4596.
(42) Saidaminov, M. I.; Mohammed, O. F.; Bakr, O. M. Low-Dimensional-Networked Metal Halide Perovskites: the Next Big Thing. *ACS Energy Lett.* **2017**, *2*, 889−896.
(43) Chen, Y.; Sun, Y.; Peng, J.; Tang, J.; Zheng, K.; Liang, Z. 2D Ruddlesden−Popper Perovskites for Optoelectronics. *Adv. Mater.* **2018**, *30*, 1703487.
(44) Smith, I. C.; Smith, M. D.; Jaffe, A.; Lin, Y.; Karunadasa, H. I. Between the Sheets: Postsynthetic Transformations in Hybrid Perovskites. *Chem. Mater.* **2017**, *29*, 1868−1884.

DOI: 10.1021/acs.jpcc.8b01164
J. Phys. Chem. C XXXX, XXX, XXX−XXX

(45) Li, Y.; Zheng, G.; Lin, C.; Lin, J. Synthesis, Structure and Optical Properties of Different Dimensional Organic−Inorganic Perovskites. *Solid State Sci.* **2007**, *9*, 855−861.
(46) Calabrese, J.; Jones, N. L.; Harlow, R. L.; Herron, N.; Thorn, D. L.; Wang, Y. Preparation and Characterization of Layered Lead Halide Compounds. *J. Am. Chem. Soc.* **1991**, *113*, 2328−2330.
(47) Papavassiliou, G. C.; Patsis, A. P.; Lagouvardos, D. J.; Koutselas, I. B. Spectroscopic Studies of $(C_{10}H_{21}NH_3)_2PbI_4$, (CH_3NH_3)-$(C_{10}H_{21}NH_3)_2Pb_2I_7$, $(CH_3NH_3)PbI_3$, and Similar Compounds. *Synth. Met.* **1993**, *57*, 3889−3894.
(48) Tabuchi, Y.; Asai, K.; Rikukawa, M.; Sanui, K.; Ishigure, K. Preparation and Characterization of Natural Lower Dimensional Layered Perovskite-Type Compounds. *J. Phys. Chem. Solids* **2000**, *61*, 837−845.
(49) Sichert, J. A.; Tong, Y.; Mutz, N.; Vollmer, M.; Fischer, S.; Milowska, K. Z.; García Cortadella, R.; Nickel, B.; Cardenas-Daw, C.; Stolarczyk, J. K.; et al. Quantum Size Effect in Organometal Halide Perovskite Nanoplatelets. *Nano Lett.* **2015**, *15*, 6521−6527.
(50) Bekenstein, Y.; Koscher, B. A.; Eaton, S. W.; Yang, P.; Alivisatos, A. P. Highly Luminescent Colloidal Nanoplates of Perovskite Cesium Lead Halide and Their Oriented Assemblies. *J. Am. Chem. Soc.* **2015**, *137*, 16008−16011.
(51) Udayabhaskararao, T.; Houben, L.; Cohen, H.; Menahem, M.; Pinkas, I.; Avram, L.; Wolf, T.; Teitelboim, A.; Leskes, M.; Yaffe, O.; Oron, D.; Kazes, M. A Mechanistic Study of Phase Transformation in Perovskite Nanocrystals Driven by Ligand Passivation. *Chem. Mater.* **2018**, *30*, 84−93.
(52) Scheele, M.; Engel, J. H.; Ferry, V. E.; Hanifi, D.; Liu, Y.; Alivisatos, A. P. Nonmonotonic Size Dependence in the Hole Mobility of Methoxide-Stabilized PbSe Quantum Dot Solids. *ACS Nano* **2013**, *7*, 6774−6781.
(53) Weiss, E. A.; Porter, V. J.; Chiechi, R. C.; Geyer, S. M.; Bell, D. C.; Bawendi, M. G.; Whitesides, G. M. The Use of Size-Selective Excitation to Study Photocurrent Through Junctions Containing Single-Size and Multi-Size Arrays of Colloidal CdSe Quantum Dots. *J. Am. Chem. Soc.* **2008**, *130*, 83−92.

DOI: 10.1021/acs.jpcc.8b01164
J. Phys. Chem. C XXXX, XXX, XXX−XXX